Structure and graph-based virtual screening in pharmacodynamics, pharmacokinetics and antioxidant activity of the Castanol B against AKR1C2 prostate cancer target

Matheus Nunes Rocha
University State of Ceará, Limoeiro do Norte
Lucas Lima Bezerra (lucas.lima@alu.ufc.br)
University Federal of Ceará
Leonardo Paes Silva
University Federal of Ceará
Francisco Wagner Queiroz Almeida-Neto
University Federal of Ceará
Márcia Machado Marinho
State University of Ceará
Hélcio Silva Santos
University State of Vale do Acaraú
Pedro Lima Neto
University Federal of Ceará
Emmanuel Silva Marinho
University State of Ceará, Limoeiro do Norte

Research Article

Keywords: Castanol B, Prostate cancer, AKR1C2 target, Pharmacokinetic and dynamics, In silico approach

Posted Date: April 14th, 2022

DOI: https://doi.org/10.21203/rs.3.rs-1543551/v1

Abstract

The Chinese chestnut cultivation represents the advance of world trade, and the consumption provides several benefits for human health. Studies reported that a Chinese chestnut has several biological activities, such as anti-inflammatory, antioxidant, and antiproliferative. The polyphenol recently isolated from Chinese chestnut known as Castanol B was analyzed through of *in silico* approach using the **ADMET** simulations, quantum calculations, molecular docking, and molecular dynamics simulations. The **ADMET** results showed that the Castanol B conjugate base is more water-soluble, then conducting a theoretical pharmacokinetic model based on a great intestinal permeability and great metabolic stability, showing an antiproliferative activity with low toxic response to the host. The quantum calculations indicated that Castanol B acts by the HAT mechanism; besides, the anion carboxylate microspecies showed better thermodynamic favoring gas and water phases. The molecular docking results showed the highest potential interaction between the Aldo-keto reductase family 1 member C2 (AKR1C2) receptor with the compound analyzed, highlighted for the Castanol B and Castanol B conjugate base. Finally, the molecular dynamics results indicated that the Castanol B conjugate base showed high stability and the highest potential of interactions during the simulations. Therefore, this compound presented might potentially be used to treat prostate cancer.

Introduction

The Chinese chestnut is widely present and commercialized in the Asiatic continent and is well known for its nutritional value and contribution to human health [1]. This chestnut is very common in China and may be found in high quantities in Korea. Furthermore, have oblong-lanceolate leaves, coarsely toothed, dark green (5–8 cm long), and pubescent below [2].

Research indicated diverse benefits with the chestnut consumption acting with heat stress relievers [3], have anti-inflammatory propriety and anti-cancer [4]. Furthermore, this chestnut has phenolic compounds that act with antioxidants [5–8], for example, the polyphenolic biphenyl compound isolated of chestnut recently for researches Chinese – the 3',4'-trihydroxy-3-carboxyl-bifenyl or Castanol B (Fig. 1) – with activity-related in the inhibition of cellular proliferation and the increase of apoptosis of hepatoma cells [4].

Studies about antioxidant activity naturally have received prominence in the world scientific community. The antioxidant effect is denominated by the action of free radical combat, such as ·OH and ·O2. Antioxidants are substances that delay or inhibit the oxidation of the subtract utilized in the free radical combat, contributing to the balance maintained in the organism, preventing the oxidation and inactivation of macromolecules, and consequently, possible pathologies harmful effects on health [9].

Given the antiproliferative activity of Castanol B in tumor cells is essential the planning of the specific action mechanism [4]. It is valid to highlight that the antioxidants, especially those extracted through functional food sources, constitute a promising strategy for prostate cancer prophylaxis [10]. A recent

study indicated the presence of antioxidant response in synergistic processes against Aldo-keto reductase (AKR1C) expressions in the antiproliferative activity of tumor cells. According to the author, the inhibition of AKR1C may potentialize the action of chemotherapy against cancer cell lines, leukemia, and colorectal cancer [11].

Therefore, the work proposes using an *in silico* approach based on the ADMET simulations and quantum calculations to characterize the Castanol B compound in the neutral form and deprotonated form (carboxylate anion). Posteriorly, analyzed the potential interaction of these species against the AKR1C2 macromolecular target associated with prostate cancer through molecular docking and molecular dynamics simulations.

Methodology

Considering that computational chemistry has gained much notoriety and efficiency as machines have gained more potential for operational calculation speed, the application of the Kohn-Sham formalism [12] was introduced in analogy to the Hartree-Fock Eq. (1930) to perform quantum calculations. Furthermore, electronic and structural characterization results were associated with virtual screening techniques since they are techniques based on the test of similarity of the proposed chemical structure with substances present in libraries that constitute databases and computer *software* [13], as detailed below.

Pass Prediction

The molecular structure of Castanol B was drawn and submitted the prediction of activity spectrum for the substances (PASS) [14] by the similarity test with the compound of data set from PASS server Online (http://way2drug.com/passonline/). This server may quantify the activity probability (Pa) and inactivity (Pi) through experimental data of tests with animals deposited in your triage base to direct the biological activity and action mechanism of substance. In addition, the SMILES code of compound was distributed for the other tools of predictive calculations.

Virtual Screening Of Target Classes

The SMILES code of molecule was uploaded in the SwissTargetPrediction (http://www.swisstargetprediction.ch/) server and configured to estimate the top 50 of the possible biological targets of interaction intermolecular by the similarity test with active molecules (3D/2D) against the *Homo sapiens* organism deposited in the ChEMBL database.

Pka Calculation And Physicochemical Properties

The upload of structure molecular of Castanol B in the MarvinSketch (version 22.5) *software*, ChemAxon (https://chemaxon.com/products/marvin), configured to realize prevision of acid constant (pKa) based in

the empiric study of molecules similar. It is essential to check the acid nature of the molecule due to the majority fraction is determined by the pH, for example, of pH blood in standard 7.4. Besides, the *software* was utilized to calculate the other physical-chemical properties dependent on pH, such as structural optimization by the calculation of force field molecular of Merck (MMFF94) (Eq. 1) [15], visually inspected by Avogadro *software* [16], as well the relative lipophilicity (logP and logD), molecular weight (MW), acceptors and donors of H-bond (HBA and HBD), and topological polar surface area (TPSA).

$$E = \sum k_b \left(r - r_0 \right)^2$$

(1)

where kb is the force constant present between two atomic nuclei separated by a bond of distance r – r_0, and the sum includes the individual contributions of each bond in the molecule. This step involves a better favoring for future geometric optimizations with more machine resources, due to a better conduction of less energy to what we call a local minimum. Considering that, throughout the optimization, the energy passes through several energy minima that do not match the global minimum energy of the molecule, it is necessary to carry out the pre-DFT step, so that the calculation tends to converge to conformations that correspond at the lowest possible energy.

Structural Characterization Of Castanol B

The structure of 3',4'-trihydroxy-3-carboxyl-bifenyl (Castanol B) was optimized through Density Functional of Theory (DFT) using the B3LYP hybrid functional [17, 18] and the 6–31 + G(d,p) basis-set [14], implemented by the ORCA 4.1.1 [19] *software*. Posteriorly, these optimized structures were checked for the absence of negative frequencies. The simulations were realized in the neutral form and deprotonated form (carboxylate anion) of compound. Besides, the simulations were performed in vacuum and water solvent described by the CPCM (Conductor-like Polarizable Continuum Model) model.

Considerations On The Use Of Enthalpy In The Process

Obtaining the intrinsic enthalpy of the molecule is necessary to calculate the BDE. The calculation of vibrational frequency gives us this data on the total enthalpies of the species. To estimate the internal energy (U), it is denoted that U(X) = E0 + ZPE + Etrans + Erot + Evib, where E0 is the calculated total electronic energy, ZPE stands for zero-point energy, Etrans, Erot and Evib are the translational, rotational and vibrational contributions to the enthalpy, respectively. From classical thermodynamics, we understand that H = U + PV. However, H = U + Kb-T is used for thermal correction of the isolated molecule, Kb being the Boltzmann constant. Finally, Kb-T represents the term PV (work) and is added to convert energy into enthalpy.

Overall, the negative variation of Gibbs free energy is a criterion governing the favorability of a process (be it a chemical reaction) to happen thermodynamically. Therefore, in the process at constant temperature and pressure, follow Eq. 2:

$$\Delta_r G = \Delta_r H - T\Delta_r S$$

(2)

However, in the study of antioxidant mechanisms, the value $T\Delta_r S$ has a relatively minute absolute value compared to the value of $\Delta_r H_r H$, which results in a change of a few tenths on the kcal/mol scale. Then, the entropic contribution can be ruled out. Thus, the mechanism is governed by the entropic value of the process.

Calculation Of Antioxidant Potential

Over the description of the HAT, SET-PT and SPLET mechanisms, the equations to obtain energy parameters follow:

BDE: Bond dissociation enthalpy, the parameter used in HAT.

$$BDE = H(ArO\bullet) + H(H\bullet) - H(ArOH)$$

(3)

IP: Ionizing potential, the first parameter used in SET-PT.

$$IP = H(ArOH^{+}\bullet) + H(e^{-}) - H(ArOH)$$

(4)

PDE: Proton dissociation enthalpy, the second parameter used in SET-PT.

$$PDE = H(ArO\bullet) + H(H^{+}) - H(ArOH^{+}\bullet)$$

(5)

PA: Proton affinity is the first parameter used in SPLET.

$$PA = H(ArO^{-}) + H(H^{+}) - H(ArOH)$$

(6)

ETE: Electron transfer enthalpy, the second parameter used in SPLET.

$$ETE = H(ArO\bullet) + H(e^{-}) - H(ArO^{-})$$

(7)

The radical formed from the antioxidation by the 5-OH, 3'-OH, and 4'-OH sites must exhibit stability for its antioxidant action to be indeed effective. The calculated gas and solvent phase enthalpies for (H•), (e^-) and (H$^+$) were obtained from references [20, 21] with the following values: (HH•): 6.2 kJ/mol, -1050.0 kJ/mol for gas and agua respectively; (e^-): 3.1 kJ/mol, -15.1 kJ/mol gas and agua respectively; (H-): -1306.6 kJ/mol, -1310.6 kJ/mol gas and agua respectively. All energies were obtained at 298.15 K and 1 atm.

Molecular docking simulations

The aldo-keto reductase family 1 member C2 (AKR1C2) receptor identified as "AKR1C2 complex with naproxen" (PDB ID: 4JQ1) was obtained by the Protein Data Bank (PDB) repository with a resolution of 1.60 Å, determined through X-ray Diffraction, composed of two chains (A and B) based *Homo sapiens* organism, and classified as the Oxidoreductase/Oxidoreductase inhibitor. The preparation of the receptor consisted of the removal of all the residues. Posteriorly, the hydrogens polar and Gasteiger charges were added [22] by the AutoDock Tools [23] *software*. The parameters of grid box were defined to compass all the protein with values of 90 Å x 106 Å x 126 Å and (x,y,z) = (-78.861, 163.889, 233.667). Furthermore, forty independent simulations were performed obtained ten conformations for each simulation. Finally, the molecular docking simulations were performed by the AutoDock Vina [24] (version 1.1.2) using 3-way multithreading, Lamarkian Genetic Algorithm. To validate all the molecular docking simulations, the re-docking technique was realized using the same parameters of the grid box for the (2S)-2-(6-methoxynaphthalen-2-yl)propanoic acid (Naproxen or NPS), co-crystallized ligand in the AKR1C2 receptor.

Molecular dynamics simulations

All the molecular dynamics (MD) simulations were realized with the Gromacs (GROningen MAchine for Chemical Simulation) [25] software implemented with the CHARMM27 [26] force field. The best-docked pose of each ligand in the receptor was utilized as the starting point for MD simulations. First, the (2S)-2-(6-methoxynaphthalen-2-yl) propanoic acid (NPS), Castanol B (CBN), and Castanol BA (CBA) parameters used in the MD simulations were obtained through the SwissParam [27] server. Next, the water molecules described by the TIP3P model [28] and five Cl^- ions were added for solvation and neutralization of the system, respectively. Posteriorly, the geometry of the system was realized through the *steepest descent* [29] and *conjugate gradient* [30] algorithms, both with 10 kJ mol^{-1} nm^{-1} of energy tolerance and 10^5 steps. The equilibrium dynamics were divided into two steps and simulated in 1 ns each step. First, the ensemble NVT was performed with a V-rescale [31] thermostat at a temperature of 310 K, followed by the ensemble NPT with Parrinello-Rahman [32] barostat with a 1.0 bar of pressure. Finally, the MD production step was simulated in 60 ns by Leap-Frog [33] integrator with the same temperature and pressure utilized in the equilibrium dynamics.

Calculation Of Physicochemical Properties And Drug-likeness

The physical-chemical properties were applicated in Eq. 8 to estimate the quantitative estimation of drug-likeness (QED) included in the ADMETlab (https://admetmesh.scbdd.com/) 2.0 server.

$$QED = exp\left[\frac{1}{n}\left(\sum_{i=1}^{n} lndi\right)\right]$$

(8)

The summation of the number properties (*n*) that include MW, logP, HBA, HBD, TPSA, Rotb, Number of Aromatic Rings (NAR), and reactive molecular fragments within the ideal spectrum (*di*) established by the “rule of five” of Lipinski [34], Veber rule [35], of influence of aromatic rings [36], and the Pan-Assay Interference Structures (PAINS) analysis [37], constitute a score ranging from 0 (Poor drug-likeness) to 1 (Good drug-likeness). The prediction was supported by the Pfizer-MultiParameter Optimization (Pf-MPO) algorithm present in the Marvin Sketch *software* that considered the individual contribution of physicochemical properties to relation the lipophilicity, molecular size, ionization with the alignment between the pharmacokinetic attributes of Castanol B, such as permeability apparent (Papp), efflux by the P-glycoprotein (P-gp), and intrinsic hepatic clearance ($CL_{int,u}$), where the score of Pf-MPO > 4 indicate a high satisfaction of physicochemical conditions:

- Low lipophilicity (logP ≤ 3 and logD ≤ 2);
- Low basicity (H-bond donors < 1 and most basic pKa ≤ 8);
- Larger size and polarity than active substances in the central nervous system (CNS) (MW ≤ 360 g/mol with the TPSA 40 ~ 90 Å²).

In Silico Adme-tox Properties

The physicochemical properties calculated in the MarvinSketch (version 22.5) *software* were associated with the predictive models of absorption, distribution, metabolism, excretion (ADME), and toxicity based on machine learning servers available online to estimate the pharmacokinetic descriptors. The graphics estimates were adapted from [40] through Spreadsheets *software* WPS Office (https://www.wps.com/).

Estimate Of Oral Absorption And Metabolic Stability

The properties calculations of MW and lipophilicity dependent on the majority microspecies in pH 7.4 (logD at pH 7.4) were plotted in the Golden Triangle graph [41] to evaluate the space physicochemical favorable for a good oral absorption and metabolic stability of Castanol B that the satisfy the

pharmacokinetic attributes of passive permeability and hepatic clearance of the Pfizer classification system.

Estimate Of Permeability And Bioavailability

The permeability and bioavailability properties were predicted by the consensus analysis of ADMETlab 2.0 (https://admetmesh.scbdd.com/), AdmetSAR 2.0 (http://lmmd.ecust.edu.cn/admetsar2/), and the SwissADME (http://www.swissadme.ch/) servers, including the prediction of human intestinal absorption (HIA), P-gp substrate and penetration blood-brain barrier (BBB) by the alignment between the properties of relative lipophilicity (WlogP) and polarity (TPSA), and pharmacokinetic descriptors as the permeability apparent (Papp), oral bioavailability (*F*), the volume of distribution and Plasma Protein Binding (PPB). The prediction was supported by the statistical regressions based on the structure-activity relation (QSAR) of the ADMET Prediction Service server (http://qsar.chem.msu.ru/admet/) that the generated distribution maps to estimate the relative bioavailability by the HIA% and permeability in the BB by the permeation coefficient blood→brain (logBB).

Site Of Metabolism, Clearance And Toxic Effects

The bidimensional structure of Castanol B was submitted to the similarity test with the metabolized substructures by the isoforms of cytochrome P450 (CYP450) in the phase I metabolism and by the UDP glucuronosyltransferase (UGT) in the phase II metabolism of XenoSite server (https://swami.wustl.edu/xenosite). The results were converted in probability 2D maps and supported by the inhibition predictions of CYP450 majorities (2C9, 2D6 e 3A4), and the estimate of $CL_{int,u}$ of teste that the match the ADMETlab 2.0 (https://admetmesh.scbdd.com/), AdmetSAR 2.0 (http://lmmd.ecust.edu.cn/admetsar2/), and SwissADME (http://www.swissadme.ch/) servers.

Prediction Of The Herg-liability

The structural contributions potentially cardiotoxic were estimated through the library of molecular fragments that inhibit hERG (the human Ether-a-go-go-Related Gene) ion transport channels from the online server Pred-hERG 4.2 (http://predherg.labmol.com.br/) and supported by the QSAR regression of ADMET Prediction Service (http://qsar.chem.msu.ru/admet/) that the esteemed the affinity constant (pKi) with the target, as the prediction method of the cardiotoxic response of Castanol B.

Prediction Of Acute Toxicity And Environmental Toxicity

To estimate acute oral toxicity was utilized the predictive models of lethal dose (LD_{50}) in mice and lethal concentration (LC_{50}) in fish through the Fathead Minnow model and inhibition growth (IGC_{50}) of

protozoan species *Tetrahymena pyriformis* as an estimate of antiproliferative effect using the AdmetSAR 2.0 (http://lmmd.ecust.edu.cn/admetsar2/) and pkCSM (http://biosig.unimelb.edu.au/pkcsm/) servers. Furthermore, the results were reinforced by the QSAR regressions based on Quantitative Neighbourhoods of Atoms (*QNA*) descriptors of the GUSAR Online (http://www.way2drug.com/gusar/) server for the same models.

Results And Discussion

Pass Analysis

The activity spectra prediction results for the substances (PASS) were registered for the activity biological probability (Pa) greater than 0.7 (Table S1) and distributed in the graph of Fig. 2a for the relevant activities for this study. The results showed an activity probability (Pa) in the value of 0.571 of Castanol B act as the free radicals scavenger due to the antioxidant effect is denominated by the action of combat free radicals [42]. Besides, the high probability estimated at 0.96 of the compound inhibits Chlordecone reductase, available as Aldo-Keto Reductase (AKR1C2) with code PDB ID:4JQ1. Therefore, assuming that PASS analyzes may lead the molecular docking simulations, the docking protocol was established against the AKR1C2 target associated with prostate cancer [43, 44]. Furthermore, the teste showed a degree of probability of 0.522 that Castanol B may act as an anti-inflammatory within the spectrum of activity reported for the substance (Fig. 2a).

Virtual Screening Of Target Classes

To conduct the AKR1C2 target for the molecular docking simulations is necessary to apply screening virtual based on chemical structure aided by machine learning functions. These functions had the main goal to realize similarity tests with the ligand or not ligand structure for the series of biological targets since those targets are inside the library in a database [45]. From the similarity test with the chemical structures deposited in ChEMBL [46] with reported activity to the several biological targets of *Homo sapiens* organism, it was possible to observe that Castanol B tends to perform around 32% of intermolecular interactions with enzymes, highlighting the similarity with at least 12 two-dimensional structures that were interacting with the AKR1C1 (ID: CHEMBL5905) and AKR1C2 (ID: CHEMBL5847) target, and with at least six structures three-dimensional to interact with the AKR1C3 (ID: CHEMBL4681), as showed the graph of Fig. 2b. In addition, the substance showed an affinity with others targets, such as lyases (14%), proteases (10%), ion channels (8%) and kinases (8%).

Estimate Of Major Microspecies By The Pka Calculation

The pKa of Castanol B is unknown due to the be molecule newly discovered. In the graph of Fig. 2c is possible to observe the microspecies distribution of Castanol B, where the pKa estimate value in the order of 3.77 associated with the hydroxyl H-bond donor of group carboxyl (COO−H), suggests the presence of

50% of specie neutral and 50% of deprotonated species in pH of 3.77. Besides, the analysis suggests that the equilibrium chemical of Castanol B moves in the direction of formation of the carboxylate group (COO^-) with the increase of pH, where a relative concentration of 97.25% is noted conjugated base in pH 7.4, as the majority microspecies.

Structural Optimization Of The Castanol B

Regarding the calculation of radicals, it is of fundamental importance to pay attention to the multiplicity of the molecule since, in the process, it will lose one unpaired electron in its highest energy occupied orbital (HOMO), thus forming the semi-occupied orbital (SOMO), generating the antioxidant radical. Thus, the total spin check (S^2) for the neutral molecule should be equal to 1 (singlet), and for the radicals, it should be around 0.75 (duplet) [47].

Castanol B presents in its structure a biphenyl, with a carboxyl group in one of its rings. When treating its geometry in classical mechanics, its structure generated a twist between the rings, differing from the initial structure designed entirely planar. With the twist of -140° on the carbons connecting the rings, the Marvin software identified the most stable conformations for the neutral (Fig. 3a) and anionic (Fig. 3b) chemical structures. The next step was to perform the optimization via DFT using the software ORCA 4.1.1. The optimization via DFT provided us not only with the optimized geometry by quantum mechanics but also the thermochemical indices (internal energy, enthalpy, entropy, Gibbs energy), the energies of HOMO and LUMO boundary orbitals, dipole moment and, among others, shown in Fig. 3c for the neutral species and Fig. 3d for the conjugate base.

Table 1
Values were calculated by the ORCA software, for Castanol B (neutral and carboxylate anion), in gaseous form.

Property	COOH	COO^-
Internal Energy	-876.845299 Eh	-876.291030 Eh
Enthalpy	-876.844354 Eh	-876.29008582 Eh
Entropy	0.000193 Eh	0.000144 Eh
Gibbs free energy	-876.901964 Eh	-876.347607 Eh
HOMO	-0.202103 Eh	-0.032883 Eh
LUMO	-0.046139 Eh	0.089418 Eh
Dipole moment	2.05273 Debye	15.87698 Debye

Antioxidant Potential

The calculations were initially performed in a vacuum, to study the antioxidant potential. Furthermore, to obtain the BDE of all sites, the hydrogens are removed from the site one wants to calculate. Then the same procedure is performed in water solvent (ε = 80.4). It is worth noting that the solvation factor is a crucial interfering factor in molecular chemical properties. BDE is a simple mechanism of the three discussed, consisting only of the direct abstraction of the radical hydrogen from the antioxidant molecule. Because Castanol B has three possible hydroxyls for the mechanism to occur, following data will compare which site is more favorable for it to occur, comparing simultaneously with the Castanol B carboxylate anion sites.

According to the plot in Fig. 4a and Fig. 4b, the BDE of the oxidizing site molecule 4'-OH has the lowest value. Considering the 4'-OH site and the resonance factor, common in aromatic compounds for radical stabilization, the radical formed forms an intramolecular hydrogen bond at the site in question, further stabilizing the radical formed. According to the calculated BDE, whether in the gas phase or in aqueous media, the HAT mechanism shows better efficiency when the molecule is a carboxylate anion, resulting in lower BDE ratios in gas and water 63 and 69.7 kcal/mol, respectively.

The leading indicator to be analyzed in the SET-PT mechanism is the IP. According to the plot in Fig. 4c, the best ionization potential is of the carboxylate anion molecule 66.07 kcal/mol in the gas phase, increasing with the solvent factor. This can be explained by the solvation of the water around the molecule. As a result, stabilization of the energy of the initial carboxylate anion occurs. When forming the "radical cation", the molecule becomes neutral. However, the IP value is higher than the parameter (BDE), which can say that there is less possibility for SET-PT to occur.

The PDE values are given in the data in Fig. 5a and Fig. 5b. The 4'-OH site presents the lowest values, corresponding that the SET-PT mechanism favors it if it happens. On the other hand, the carboxylate anion in an aqueous medium presented the best results. However, adding to the previous step (IP), the SET-PT becomes quite energetic, reaching 128.39 kcal/mol (value referring to IP + PDE) when compared to the BDE (69.72 kcal/mol, in the same conditions) of the HAT mechanism.

SPLET is the third important mechanism studied, and previous studies of phenolic compounds have confirmed the possible use in the presence of polar solvents [48, 49]. Furthermore, the values of the 4'-OH site are also favored in the SPLET mechanism, standing out in the aqueous medium, where there is a drastic reduction of energies for the PA parameter (Fig. 6) corroborating with the studies already cited.

Performing a final comparison between the three mechanisms, highlighting the 4'-OH site (having the lowest values among the three phenolic hydroxyls of Castanol B), we arrive at the graphs in Fig. 7a and Fig. 7b. The HAT mechanism presents the most thermodynamically favorable data. The deprotonated castanol molecule is favored for free radical oxidation, whose values are comparable to traditional antioxidant compounds such as gallic acid, Quercetin, and others (Fig. 7c) [50].

Molecular docking

The molecular docking simulations were realized to understand the possible mechanism of action of the molecules analyzed in the AKR1C2 receptor. Figure 8 showed the affinity energy values, Root Mean Square Deviation (RMSD) values, and binding site of AKR1C2-NPS (re-docking), AKR1C2-CBN, and AKR1C2-CBA complexes. The AKR1C2-NPS complex (Fig. 8) registered the affinity energy value − 8.7 kcal/mol and RMSD value of 0.9030 Å. Besides, this complex showed one hydrogen bond with Ser 217 amino acid and eight hydrophobic interactions with the Tyr 24, Tyr 55, Tyr 216, Ser 217, Leu 268, and Leu 306 residues. The CBN ligand (Fig. 8) showed the affinity energy value of -9.0 kcal/mol, RMSD value of 1.2800 Å and interacted with the AKR1C2 receptor through five hydrogen bonds (Asp 366, His 433, Ser 482, Asn 483, and Gln 506 amino acids), two hydrophobic interactions (Asp 366 and Leu 622 residues), and one π-stacking (Tyr 532). Furthermore, this ligand showed the charge center with the His 538 amino acid. The AKR1C2-CBA complex (Fig. 8) registered an -9.1 kcal/mol affinity energy value and an RMSD value of 1.2890 Å. Besides, This complex presented six hydrogen bonds (Ser 482, Asn 483, Tyr 532, Ser 533, and Gln 506 amino acids), one hydrophobic interaction (Tyr 532 residue), one π-stacking (Leu 622 amino acid), one charge center (His 538 residue).

The molecular docking results indicated that all ligands showed a high potential interaction with the AKR1C2 receptor due to better affinity energy values than the affinity energy standard value of -6.0 kcal/mol [51]. Furthermore, all complexes registered RMSD values below 2.0 Å [52]. However, only the AKR1C2-CBN and AKR1C2-CBA complexes were used in the molecular dynamics simulation due to the affinity energy values similars.

Molecular dynamics

The MD simulations analyzed the stability of complexes formed by the best-pose from molecular docking calculations. The Root Mean Square Deviation (RMSD) was performed using the C-α of the receptor as the reference for the AKR1C2-CBN (Fig. 9a) and AKR1C2-CBA (Fig. 9b) complexes. The AKR1C2-CBN complex showed the average RMSD value of 1.53 Å and reached the equilibrium from 30 ns in the two MD simulations. However, in the third MD simulation was registered average RMSD in the value of 2.76 Å considered above the standard value (RMSD < 2.0 Å) [52]. The AKR1C2-CBA complex registered the average RMSD in the value of 1.44 Å and reached the equilibrium from 30 ns in the three replicates. Therefore, the RMSD results indicated that the CBA ligand showed interactions more stable with the AKR1C2 receptor than the CBN ligand. The Interaction Potential Energy (IPE) analysis was realized only from the interval time that the complexes reached equilibrium.

The IPE analysis was performed by summing short-range energies Coulomb and Lennard-Jones between the AKR1C2 receptor with the CBN and CBA ligands. Table 2 showed that the AKR1C2-CBN and AKR1C2-CBA complexes registered IPE values of -198.4660 kJ mol^{-1} (± 33.4447) and − 278.0350 kJ mol^{-1} (± 32.6707), respectively. Besides, the IPE analysis showed the contribution of each residue in the AKR1C2 receptor with a maximum distance of 5.0 Å of ligand analyzed. The AKR1C2-CBN complex registered IPE values of -4.3478 kJ mol^{-1} (± 2.8673), -15.5050 kJ mol^{-1} (± 14.6606), -1.1295 kJ mol^{-1} (± 1.4342), -19.3830 kJ mol^{-1} (± 2.8340), -16.8722 kJ mol^{-1} (± 3.6573), -2.2047 kJ mol^{-1} (± 1.8664), -2.4042 kJ

mol^{-1} (± 1.0490), -6.8459 kJ mol^{-1} (± 5.8047), -0.7878 kJ mol^{-1} (± 1.0076), -10.3324 kJ mol^{-1} (± 2.6303), -6.8529 kJ mol^{-1} (± 2.3461), and – 3.5326 kJ mol^{-1} (± 1.9567) with the Gly 22, Asp 50, His 117, Tyr 216, Ser 217, Ala 218, Leu 219, Ser 221, His 222, Leu 268, Ala 269, and Leu 306 amino acids.

The AKR1C2-CBA complex showed the IPE values of -6.6544 kJ mol^{-1} (± 1.3855), -76.5398 kJ mol^{-1} (± 7.1892), -11.8891 kJ mol^{-1} (± 4.8265), -34.3912 kJ mol^{-1} (± 5.6294), -18.5110 kJ mol^{-1} (± 9.0857), -4.5020 kJ mol^{-1} (± 1.6759), -3.6080 kJ mol^{-1} (± 4.1628), -18.6121 kJ mol^{-1} (± 16.5207), -8.1960 kJ mol^{-1} (± 10.0727), -4.9431 kJ mol^{-1} (± 3.1764), -5.7373 kJ mol^{-1} (± 2.007), and – 2.8957 kJ mol^{-1} (± 1.6507) with the Gly 22, Asp 50, His 117, Tyr 216, Ser 217, Ala 218, Leu 219, Ser 221, His 222, Leu 268, Ala 269, and Leu 306 amino acids. Therefore, the IPE results indicated that the CBN and CBA ligands interacted most strongly with the Asp 50, His 117, Tyr 216, Ser 217, Ser 221, and Leu 268 residues, highlighted especially the CBA ligand.

Table 2

Interaction Potential Energy (IPE) (in kJ mol^{-1}) between the residues of the AKR1C2 receptor with the CBN and CBA ligands, with standard deviation.

Residue	IPE (kJ mol^{-1})	
	CBN	CBA
Gly 22	-4.3478 (± 2.8673)	-6.6544 (± 1.3855)
Asp 50	-15.5050 (± 14.6606)	-76.5398 (± 7.1892)
His 117	-1.1295 (± 1.4342)	-11.8891 (± 4.8265)
Tyr 216	-19.3830 (± 2.8340)	-34.3912 (± 5.6294)
Ser 217	-16.8722 (± 3.6573)	-18.5110 (± 9.0857)
Ala 218	-2.2047 (± 1.8664)	-4.5020 (± 1.6759)
Leu 219	-2.4042 (± 1.0490)	-3.6080 (± 4.1628)
Ser 221	-6.8459 (± 5.8047)	-18.6121 (± 16.5207)
His 222	-0.7878 (± 1.0076)	-8.1960 (± 10.0727)
Leu 268	-10.3324 (± 2.6303)	-4.9431 (± 3.1764)
Ala 269	-6.8529 (± 2.3461)	-5.7373 (± 2.007)
Leu 306	-3.5326 (± 1.9567)	-2.8957 (± 1.6507)

Physicochemical Properties And Drug-likeness

The QED (Eq. 8) application resulted in a drug-likeness score in the value of 0.61, indicating that Castanol B satisfies the most physicochemical conditions of drug-similarity due to the weight molecular is of 246.22 g/mol and the logP of 2.37 showed that the substance is small and petite lipophilic, while the total of 2 rotatable bonds (Rotb) characterize its semi-rigid structure, passing through the filter that matches the criteria if drug-likeness of Lipinski [34] and Veber [35]: logP ≤ 5, MW ≤ 500 g/mol, H-bond acceptors (HBA) ≤ 10, H-bond donors (HBD) ≤ 5, polarity (TPSA) ≤ 140 Å², and Rotb ≤ 10 (Table 3). However, the PAINS filter detected a structural alert associated with the Catechol fragment, revealing the high polarity of Castanol B.

When applicated in the Pf-MPO algorithm is observed that the quantity of H-bond donors associated with the 3'-OH, 4'-OH, 5-OH, and COOH groups, not within the spectrum formed by the physicochemical limits, evidenced in the radar of Fig. 10a by contributed heavily for the high polarity topological of Castanol B available in 97.99 Å². However, the substance is in a low lipophilicity spectrum, besides being bigger and more polar than the active substances in CNS of Pfizer database (MW ≤ 360 g/mol with TPSA > 40 Å²) [38]. Therefore, the Pf-MPO score of 4.73 suggests that the alignment between the physicochemical properties leads to an optimization of pharmacokinetic parameters of Castanol B (Table 3).

Table 3
Physicochemical properties are calculated and applied to drug-likeness filters and estimates.

Parameter	Property	Value
Physicochemical properties	pKa (most acid)	3.77
	pKa (most basic)	-6.03
	logP	2.37
	logD	-0.92
	MW	246.22 g/mol
	HBA	5
	HBD	4
	TPSA	97.99 Å²
	Rotb	2
	NAR	2
Medicinal chemistry	PAINS	1 alert; Catechol_A
	Lipinski	Accepted
	Veber	Accepted
	QED	0.61
	Pf-MPO	4.73

Note: MW (Molecular weight); HBA (H-bond acceptors); HBD (H-bond donors); TPSA (Topological Polar Surface Area); Rotb (Rotatable bonds); NAR (Number of aromatic rings); PAINS (Pan Assay Interference Structures); QED (Quantitative estimate of drug-likeness); Pf-MPO (Pfizer's Multiparameter optimization).

In Silico Adme-tox Properties

Estimate oral absorption and metabolic stability

To Johnson *et al.*, [41] (Pfizer, Inc.), properties such as MW and logD replace other physicochemical properties, such as TPSA, H-bond donor/acceptor, and ionization, for being strongly used associated with the permeability and metabolic clearance of drugs. Therefore, it is possible to note that the formation of base conjugate causes a decrease in relative lipophilicity of Castanol B, available at -0.92 by the logD at pH 7.4, about intrinsic lipophilicity (logP 2.37), which aligns with the weight molecular of 246.22 g/mol, configured an optimization in the absorption and in the metabolic stability of the substance, according to

the physical-chemical space of the Pfizer database (Fig. 10b), formed by the limits of -2 < logD ≤ 5 and 200 < MW ≤ 500 g/mol.

Estimate Of Permeability And Bioavailability

The results of the ADME test between the ADMETlab 2.0, AdmetSAR 2.0, and SwissADME servers showed the correlation between the empirical decisions and pharmacokinetic descriptors of Castanol B and are inspected in Fig. 10c and Table 4. The permeability value of the Madin-Darby canine kidney cell (Papp MDCK) model in the value of 6.5×10⁻⁶ cm/s indicates moderate permeability (2.5 < Papp ≤ 10, in 10⁻⁶ cm/s), according to with the Pfizer's rating system [38]. The prediction corroborates with an empirical decision of the graph of BOILED-Egg [53], where the TPSA ensures good passive intestinal permeability; however, it prevents penetration into the CNS for being in an interval of difficult penetration in the BBB (79 < TPSA ≤ 142 Å²) (Fig. 10c).

Therefore, intestinal absorption becomes a fundamental criterion for selecting a candidate for the local action drug related to the absorbed oral dose with the molecular fraction bioavailable in the systemic circulation [54]. Although ionizable compounds showed a decrease in the oral bioavailable, as a general rule for the drugs [55], an experimental observation made by Martin [56] showed that the fraction of 56% of anionic compounds with the polarity topological of 75 ~ 150 Å² showed selective permeability in Caco-2 cells, of a test database in mice, estimating a fraction of oral bioavailable (*F*) of 0.56 for the substances with high polarity. However, according to the experimental analysis of Veber [35], the permeability attributes and drug transport decrease as the TPSA approaches 140 Å². Then, the statistical regressions of QSAR of the ADMET Prediction Service tool estimate a relative oral bioavailability of 55.37% (Fig. 11a) in the function of physicochemical space occupied with the Castanol B (75 < TPSA < 150 Å²), corroborating with the *F* of bioavailable of empirical decisions of the consensual test around of 0.55–0.56 (Table 4). At the same time, the low volume of distribution available at 0.402 L/kg indicates that the substance tends to be more distributed in blood plasma fluid than in tissues, including the BBB, where the permeability value blood→brain (log BB) in the value of -1.13 reflects the low penetrability of the compounds in the brain (Fig. 11b).

Site Of Metabolism, Clearance And Toxic Effects

The prediction of metabolism sites search reduces the selection of substrate of the isoform of CYP450 able to form secondary metabolites reactive and subjects to induce liver damage (DILI) [57]. Although the lipophilicity estimated (elogD) is a model very associated with solubility and permeability and may also estimate the metabolic stability and the resistance of the biotransformed substance [41]. The low lipophilicity estimated of Castanol B leads a pharmacologic model little likely to form secondary metabolites in the metabolism of phase I, where the value of intrinsic debugging in the value of 10.036 mL/min/kg suggests that the substance is easily excreted (Table 4). In the map of probability of Fig. 11c, the aromatic carbon at position 4 has a low probability of being hydroxylated by the CYP2A6 isoform

(phase I). However, constitute a chemical entity most susceptible to undergoing aromatic hydroxylation. Besides, it is also observed that the 3'-OH, 4'-OH, and 5-OH sites presented susceptible sites to form metabolites conjugate active from glucuronida reactions by the UGT enzyme (phase II). However, the biotransformation is barely viable (P 0.5), as shown in Fig. 11c. Therefore, the low susceptibility of Castanol B in being subtracted from the majority isoforms of CYP450 (2C9, 2D6, and 3A4) makes it a non-inhibitor to those isoenzymes with a low probability of inducing lesions to the liver (Table 4).

Table 4
Results of the consensual prediction of ADME between ADMETlab 2.0, AdmetSAR 2.0 and SwissADME databases.

Prediction	ADMETlab 2.0	AdmetSAR 2.0	SwissADME
Papp*	6.5×10⁻⁵ cm/s	+	+[a]
P-gp substrate	–	–	–
HIA	High	+	High[b]
Bioavailability, *F*	Low	+ (0.557)	0.56[a]
Volume of distribution	0.402 L/kg	n.a.	n.a.
BBB permeation	–	–	–[b]
CYP2C9 inhibitor	–	–	–
CYP2D6 inhibitor	–	–	–
CYP3A4 inhibitor	–	–	+
*Papp prediction of the Madin-Darby canine kidney cell (MDCK) model from the ADMETlab 2.0 database and adenocarcinoma colorectal cells (Caco-2) from the AdmetSAR 2.0 and SwissADME databases.			
Note: HIA (Human intestinal absorption); BBB (Blood-brain barrier) CYP (cytochrome P450); a = calculated by the method of Martin (2005); b = predicted by the BOILED-Egg graphical model. n.a. = not reported.			

Prediction Of The Herg-liability

Another prediction dependent on structural analysis is the identity of fragments molecular potentially inhibitors of hERG channels (the human Ether-a-go-go-Related Gene), a conveyor of K + ions for the cardiorespiratory system. This inhibition occasioned side effects associated with cardiotoxicity, such as cardiac arrhythmia [58, 59]. In this work, the statical regressions based on QSAR reveal the low potential cardiotoxic of Castanol B. In the map of probability 2D of Fig. 12, the contributions structural of Castanol B are susceptible to the inhibition, or not, of the channel of transport of hERG (the human Ether-a-go-go-Related Gene) ions are observed. In this channel, despite the negative effect of phenolic hydroxyls and

carboxylate group (magenta color), the sum of contribution positive associated with the aromatic ring (green color) reflects the low blocking potential hERG, where the pKi evaluated in 4.78, behind 90% of compounds of the database with the pKi values above ideal, suggests that the substance have a low affinity with the channels, resulting in a low incidence of cardiotoxicity.

Evaluation of acute toxicity and environmental toxicity

Recently, the QSAR models constitute the toxic structure database evolved into a physicochemical space that negatively encompasses molecular fragments in species environmental species such as the fish (Fathead Minnow) and the *Tetrahymena pyriformis* protozoan [60]. The analysis realized in this work suggests that Castanol B has a low toxicity incidence by ingestion and may also act as a cell antiproliferative agent. When evaluating the acute toxicity models is observed that the estimated value of lethal dose of 50% in mice (LD_{50}) in the value of 2044 mg/kg classified the substance as low toxicity class, according to reference [61], corroborating with the predicted concentration is around of 2.0 mol/kg (Table 5). Concerning the lethal concentration (LC_{50}) in environment species is observed noted that the estimated value of 1.374 mM indicates the low lethality in a tested fish population, corroborating with the values inside of domain of applicability of the QSAR model of the GUSAR online tool, while the values of IGC_{50} between the 0.3–0.6 μg/L, close to the estimated spectrum in $-\log_{10}$(mol/L), indicates that the Castanol B tends to inhibit the growth of the *Tetrahymena pyriformis* protozoan, conduces the antiproliferative model of substance (Table 5).

Table 5
Results of consensus prediction of organic toxicity and environmental toxicity models between ADMETlab 2.0, AdmetSAR 2.0 and GUSAR Online databases.

Prediction	GUSAR Online	AdmetSAR 2.0	pkCSM
LD_{50} Oral in rat	2044 mg/kg	2.032 mol/kg	1.931 mol/kg
LC_{50} Minnow*	-1.833 $\log_{10}$(mmol/L)	n.a.	1.374 mM
IGC_{50} *T. pyriformis*	1.565 $-\log_{10}$(mol/L)	0.622 μg/L	0.377 μg/L
*Prediction of positive log of lethal concentration ($\log_{10}LC_{50}$ in mmol/L) from GUSAR Online server and negative log of lethal concentration ($-\log_{10}LC_{50}$ in mM) from pkCSM server.			

Conclusion

From the initial estimate of the dominant microspecies, dependent on the pH = pKa relationship, it can be concluded that the carboxylate anion microspecies, predominant in blood pH (pH of approximately 7.4), constitutes a better antioxidant agent in relation to its acidic species, favoring a lower order of Gibbs free energy for complex formation with AKR1C2 in molecular docking tests. Thus, the chemical entity constitutes an affinity balance of greater stability in molecular dynamics tests, corroborating the target inhibition estimate at a probability of 96%, predicted in the PASS test. Furthermore, the series of tools

used for a consensual test of ADME, including graphical estimates and pharmacokinetic descriptors, was able to reach a theoretical model where the conjugate base (COO⁻) presents a more water-soluble chemical and, therefore, less susceptible to biotransformation. in the liver, indicating that the bioavailable fraction of ~ 56% is easily excreted by the kidneys, leading to antiproliferative activity with a low risk of liver damage, through resistance to the formation of reactive secondary metabolites in the hepatic system, as well as a low incidence of residual accumulation. of the substance in tissues.

Declarations

Competing Interests

The authors declared no conflict of interests.

Acknowledgements

We acknowledge financial support from FUNCAP, CNPq and CAPES. Hélcio S. dos Santos acknowledges financial support from the PQ/FUNCAP (Grant#: BP4-0172-00075.01.00/20). The authors also thank the Centro Nacional de Processamento de Alto Desempenho (CENAPAD) of the Federal University of Ceará (UFC) for providing computational resources.

References

1. Zhang L, Gao H, Baba M, et al (2014) Extracts and compounds with anti-diabetic complications and anti-cancer activity from Castanea mollissina Blume (Chinese chestnut). BMC Complement Altern Med 14:422. https://doi.org/10.1186/1472-6882-14-422
2. Warmund MR (2011) Chinese Chestnut (Castanea mollissima) as a Niche Crop in the Central Region of the United States. HortScience 46:345–347.https://doi.org/10.21273/HORTSCI.46.3.345
3. Dong S, Li H, Gasco L, et al (2015) Antioxidative activity of the polyphenols from the involucres of Castanea mollissima Blume and their mitigating effects on heat stress. Poult Sci 94:1096–1104.https://doi.org/10.3382/ps/pev101
4. Fei W, Xuan Y, Jian X, et al (2019) One New Phenolic Compound from Castanea mollissima Shells and its Suppression of HepatomaCell Proliferation and Inflammation by Inhibiting NF-κB Pathway. Int J Mol Sci 20:466.https://doi.org/10.3390/ijms20030466
5. Zhao S, Liu JY, Chen SY, et al (2011) Antioxidant Potential of Polyphenols and Tannins from Burs of Castanea mollissima Blume. Molecules 16:8590–8600.https://doi.org/10.3390/molecules16108590
6. Ogawa S, Kimura H, Niimi A, et al (2008) Fractionation and Structural Characterization of Polyphenolic Antioxidants from Seed Shells of Japanese Horse Chestnut (Aesculus turbinata BLUME). J Agric Food Chem 56:12046–12051.https://doi.org/10.1021/jf802506r
7. Vázquez G, Fontenla E, Santos J, et al (2008) Antioxidant activity and phenolic content of chestnut (Castanea sativa) shell and eucalyptus (Eucalyptus globulus) bark extracts. Ind Crops Prod 28:279–

285.https://doi.org/10.1016/j.indcrop.2008.03.003

8. You Y, Duan X, Wei X, et al (2007) Identificationof Major Phenolic Compounds of Chinese Water Chestnut and their Antioxidant Activity. Molecules 12:842–852.https://doi.org/10.3390/12040842
9. Sharma GN, Gupta G, Sharma P (2018) A Comprehensive Review of Free Radicals, Antioxidants, and Their Relationship with Human Ailments. Crit Rev Eukaryot Gene Expr 28:139–154.https://doi.org/10.1615/CritRevEukaryotGeneExpr.2018022258
10. Bhandari R, Khanna G, Kuhad A (2021) Prostate cancer and food-based antioxidants in India as plausible therapeutics. In: Cancer. Elsevier, pp 203–217
11. Penning TM, Jonnalagadda S, Trippier PC, Rižner TL (2021) Aldo-Keto Reductases and Cancer Drug Resistance. Pharmacol Rev 73:1150–1171.https://doi.org/10.1124/pharmrev.120.000122
12. Kohn W, Sham LJ (1965) Self-Consistent Equations Including Exchange and Correlation Effects. Phys Rev 140:A1133–A1138.https://doi.org/10.1103/PhysRev.140.A1133
13. da Silva Rocha SFL, Olanda CG, Fokoue HH, Sant'Anna CMR (2019) Virtual Screening Techniques in Drug Discovery: Review and Recent Applications. Curr Top Med Chem 19:1751–1767.https://doi.org/10.2174/1568026619666190816101948
14. Filimonov DA, Druzhilovskiy DS, Lagunin AA, et al (2018) Computer-aided prediction of biological activity spectra for chemical compounds: opportunities and limitation. Biomed Chem Res Methods 1:e00004.https://doi.org/10.18097/bmcrm00004
15. Halgren TA (1996) Merck molecular force field. I. Basis, form, scope, parameterization, and performance of MMFF94. J Comput Chem 17:490–519.https://doi.org/10.1002/(SICI)1096-987X(199604)17:5/6<490::AID-JCC1>3.0.CO;2-P
16. Hanwell MD, Curtis DE, Lonie DC, et al (2012) Avogadro: an advanced semantic chemical editor, visualization, and analysis platform. J Cheminform 4:17.https://doi.org/10.1186/1758-2946-4-17
17. Becke AD (2014) Perspective: Fifty years of density-functional theory in chemical physics. J Chem Phys 140:18A301.https://doi.org/10.1063/1.4869598
18. Ditchfield R, Hehre WJ, Pople JA (1971) Self-Consistent Molecular-Orbital Methods. IX. An Extended Gaussian-Type Basis for Molecular-Orbital Studies of Organic Molecules. J Chem Phys 54:724–728.https://doi.org/10.1063/1.1674902
19. Neese F (2018) Software update: the ORCA program system, version 4.0. WIREs Comput Mol Sci 8:1–6.https://doi.org/10.1002/wcms.1327
20. Rimarčík J, Lukeš V, Klein E, Ilčin M (2010) Study of the solvent effect on the enthalpies of homolytic and heterolytic N–H bond cleavage in p-phenylenediamine and tetracyano-p-phenylenediamine. J Mol Struct THEOCHEM 952:25–30.https://doi.org/10.1016/j.theochem.2010.04.002
21. Zheng Y-Z, Deng G, Guo R, et al (2019) DFT Studies on the Antioxidant Activity of Naringenin and Its Derivatives: Effects of the Substituents at C3. Int J Mol Sci 20:1450.https://doi.org/10.3390/ijms20061450

22. Yan J, Zhang G, Pan J, Wang Y (2014) α-Glucosidase inhibition by luteolin: Kinetics, interaction and molecular docking. Int J Biol Macromol 64:213–223.https://doi.org/10.1016/j.ijbiomac.2013.12.007
23. Morris GM, Huey R, Lindstrom W, et al (2009) AutoDock4 and AutoDockTools4: Automated docking with selective receptor flexibility. J Comput Chem 30:2785–2791.https://doi.org/10.1002/jcc.21256
24. Trott O, Olson AJ (2010) AutoDock Vina: Improving the speed and accuracy of docking with a new scoring function, efficient optimization, and multithreading. J Comput Chem 31:445–461.https://doi.org/10.1002/jcc.21334
25. Van Der Spoel D, Lindahl E, Hess B, et al (2005) GROMACS: Fast, flexible, and free. J Comput Chem 26:1701–1718.https://doi.org/10.1002/jcc.20291
26. MacKerell AD, Banavali N, Foloppe N (2000) Development and current status of the CHARMM force field for nucleic acids. Biopolymers 56:257–265.https://doi.org/10.1002/1097-0282(2000)56:4<257::AID-BIP10029>3.0.CO;2-W
27. Zoete V, Cuendet MA, Grosdidier A, Michielin O (2011) SwissParam: A fast force field generation tool for small organic molecules. J Comput Chem 32:2359–2368.https://doi.org/10.1002/jcc.21816
28. Jorgensen WL, Chandrasekhar J, Madura JD, et al (1983) Comparison of simple potential functions for simulating liquid water. J Chem Phys 79:926–935.https://doi.org/10.1063/1.445869
29. Arfken GB, Weber HJ, Spector D (1999) Mathematical Methods for Physicists, 4th ed. Am J Phys 67:165–169.https://doi.org/10.1119/1.19217
30. Hestenes MR, Stiefel E (1952) Methods of Conjugate Gradients for Solving. J Res Natl Bur Stand (1934) 49:409
31. Bussi G, Donadio D, Parrinello M (2007) Canonical sampling through velocity rescaling. J Chem Phys 126:014101.https://doi.org/10.1063/1.2408420
32. Nosé S, Klein ML (1983) Constant pressure molecular dynamics for molecular systems. Mol Phys 50:1055–1076.https://doi.org/10.1080/00268978300102851
33. Van Gunsteren WF, Berendsen HJC (1988) A Leap-frog Algorithm for Stochastic Dynamics. Mol Simul 1:173–185.https://doi.org/10.1080/08927028808080941
34. Lipinski CA (2004) Lead- and drug-like compounds: The rule-of-five revolution. Drug Discov Today Technol 1:337–341.https://doi.org/10.1016/j.ddtec.2004.11.007
35. Veber DF, Johnson SR, Cheng H, et al (2002) Molecular Properties That Influence the Oral Bioavailability of Drug Candidates. J Med Chem 45:2615–2623.https://doi.org/10.1021/jm020017n
36. Ritchie TJ, Macdonald SJF (2009) The impact of aromatic ring count on compound developability – are too many aromatic rings a liability in drug design? Drug Discov Today 14:1011–1020.https://doi.org/10.1016/j.drudis.2009.07.014
37. Baell JB, Holloway GA (2010) New Substructure Filters for Removal of Pan Assay Interference Compounds (PAINS) from Screening Libraries and for Their Exclusion in Bioassays. J Med Chem 53:2719–2740.https://doi.org/10.1021/jm901137j

38. Wager TT, Hou X, Verhoest PR, Villalobos A (2016) Central Nervous System Multiparameter Optimization Desirability: Application in Drug Discovery. ACS Chem Neurosci 7:767–775.https://doi.org/10.1021/acschemneuro.6b00029
39. Lima J dos R, Ferreira MKA, Sales KVB, et al (2021) Diterpene Sonderianin isolated from Croton blanchetianus exhibits acetylcholinesterase inhibitory action and anxiolytic effect in adult zebrafish (Danio rerio) by 5-HT system. J Biomol Struct Dyn 1–16.https://doi.org/10.1080/07391102.2021.1991477
40. Ritchie TJ, Ertl P, Lewis R (2011) The graphical representation of ADME-related molecule properties for medicinal chemists. Drug Discov Today 16:65–72.https://doi.org/10.1016/j.drudis.2010.11.002
41. Johnson TW, Dress KR, Edwards M (2009) Using the Golden Triangle to optimize clearance and oral absorption. Bioorganic Med Chem Lett 19:5560–5564.https://doi.org/10.1016/j.bmcl.2009.08.045
42. Galano A, Raúl Alvarez-Idaboy J (2019) Computational strategies for predicting free radical scavengers' protection against oxidative stress: Where are we and what might follow? Int J Quantum Chem 119:e25665.https://doi.org/10.1002/qua.25665
43. Al-Tamimi A-MS, Mary YS, Hassan HM, et al (2018) Study on the structure, vibrational analysis and molecular docking of fluorophenyl derivatives using FT-IR and density functional theory computations. J Mol Struct 1164:172–179.https://doi.org/10.1016/j.molstruc.2018.03.070
44. Zeng C-M, Chang L-L, Ying M-D, et al (2017) Aldo–Keto Reductase AKR1C1–AKR1C4: Functions, Regulation, and Intervention for Anti-cancer Therapy. Front Pharmacol 8:1–9.https://doi.org/10.3389/fphar.2017.00119
45. Li H, Sze K, Lu G, Ballester PJ (2021) Machine-learning scoring functions for structure-based virtual screening. WIREs Comput Mol Sci 11:1–21.https://doi.org/10.1002/wcms.1478
46. Mendez D, Gaulton A, Bento AP, et al (2019) ChEMBL: Towards direct deposition of bioassay data. Nucleic Acids Res 47:D930–D940.https://doi.org/10.1093/nar/gky1075
47. Jensen F (2017) Introduction to computational chemistry, 1st ed. John wiley & sons, England
48. Vagánek A, Rimarčík J, Dropková K, et al (2014) Reaction enthalpies of OH bonds splitting-off in flavonoids: The role of non-polar and polar solvent. Comput Theor Chem 1050:31–38.https://doi.org/10.1016/j.comptc.2014.10.020
49. Wang G, Xue Y, An L, et al (2015) Theoretical study on the structural and antioxidant properties of some recently synthesised 2,4,5-trimethoxy chalcones. Food Chem 171:89–97.https://doi.org/10.1016/j.foodchem.2014.08.106
50. Guitard R, Nardello-Rataj V, Aubry J-M (2016) Theoretical and Kinetic Tools for Selecting Effective Antioxidants: Application to the Protection of Omega-3 Oils with Natural and Synthetic Phenols. Int J Mol Sci 17:1220.https://doi.org/10.3390/ijms17081220
51. Shityakov S, Foerster C (2014) In silico predictive model to determine vector-mediated transport properties for the blood-brain barrier choline transporter. Adv Appl Bioinforma Chem 23.https://doi.org/10.2147/AABC.S63749

52. Yusuf D, Davis AM, Kleywegt GJ, Schmitt S (2008) An Alternative Method for the Evaluation of Docking Performance: RSR vs RMSD. J Chem Inf Model 48:1411–1422.https://doi.org/10.1021/ci800084x
53. Daina A, Zoete V (2016) A BOILED-egg to predict gastrointestinal absorption and brain penetration of small molecules. ChemMedChem 11:1117–1121.https://doi.org/10.1002/cmdc.201600182
54. Newby D, Freitas AA, Ghafourian T (2015) Decision trees to characterise the roles of permeability and solubility on the prediction of oral absorption. Eur J Med Chem 90:751–765.https://doi.org/10.1016/j.ejmech.2014.12.006
55. Pires DE V., Kaminskas LM, Ascher DB (2018) Prediction and Optimization of Pharmacokinetic and Toxicity Properties of the Ligand. In: Computational Drug Discovery and Design. Humana Press, New York, NY, pp 271–284
56. Martin YC (2005) A Bioavailability Score. J Med Chem 48:3164–3170.https://doi.org/10.1021/jm0492002
57. Yu K, Geng X, Chen M, et al (2014) High daily dose and being a substrate of cytochrome P450 enzymes are two important predictors of drug-induced liver injury. Drug Metab Dispos 42:744–750.https://doi.org/10.1124/dmd.113.056267
58. Braga RC, Alves VM, Silva MFB, et al (2015) Pred-hERG: A Novel web-Accessible Computational Tool for Predicting Cardiac Toxicity. Mol Inform 34:698–701. https://doi.org/10.1002/minf.201500040
59. Cavalluzzi MM, Imbrici P, Gualdani R, et al (2020) Human ether-à-go-go-related potassium channel: exploring SAR to improve drug design. Drug Discov Today 25:344–366.https://doi.org/10.1016/j.drudis.2019.11.005
60. Tinkov O, Polishchuk P, Matveieva M, et al (2021) The Influence of Structural Patterns on Acute Aquatic Toxicity of Organic Compounds. Mol Inform 40:2000209.https://doi.org/10.1002/minf.202000209
61. Diaza RG, Manganelli S, Esposito A, et al (2015) Comparison of in silico tools for evaluating rat oral acute toxicity. SAR QSAR Environ Res 26:1–27.https://doi.org/10.1080/1062936X.2014.977819

Figures

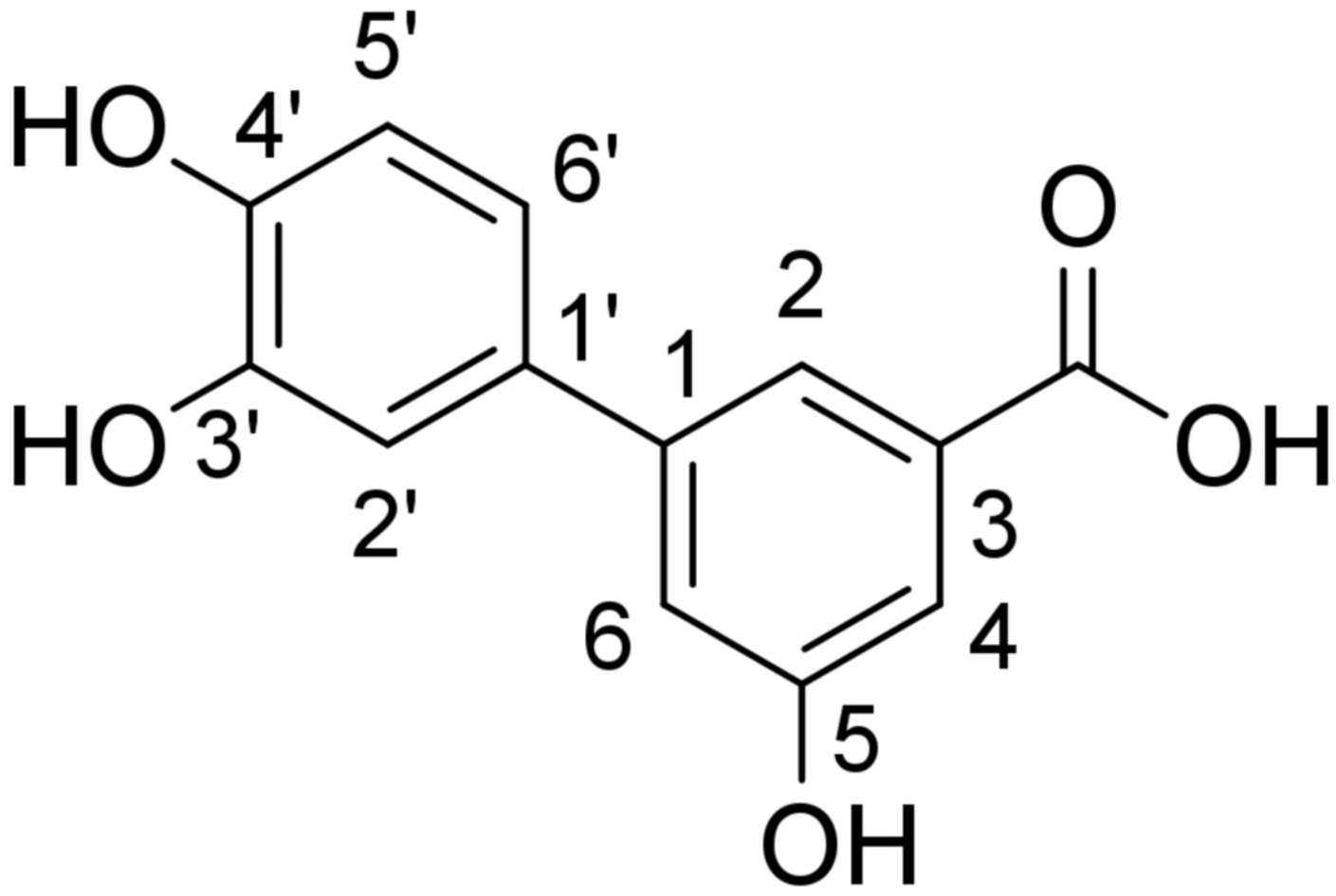

Figure 1

The two-dimensional structure of Castanol B with sites on aromatic rings is highlighted with IUPAC numbering.

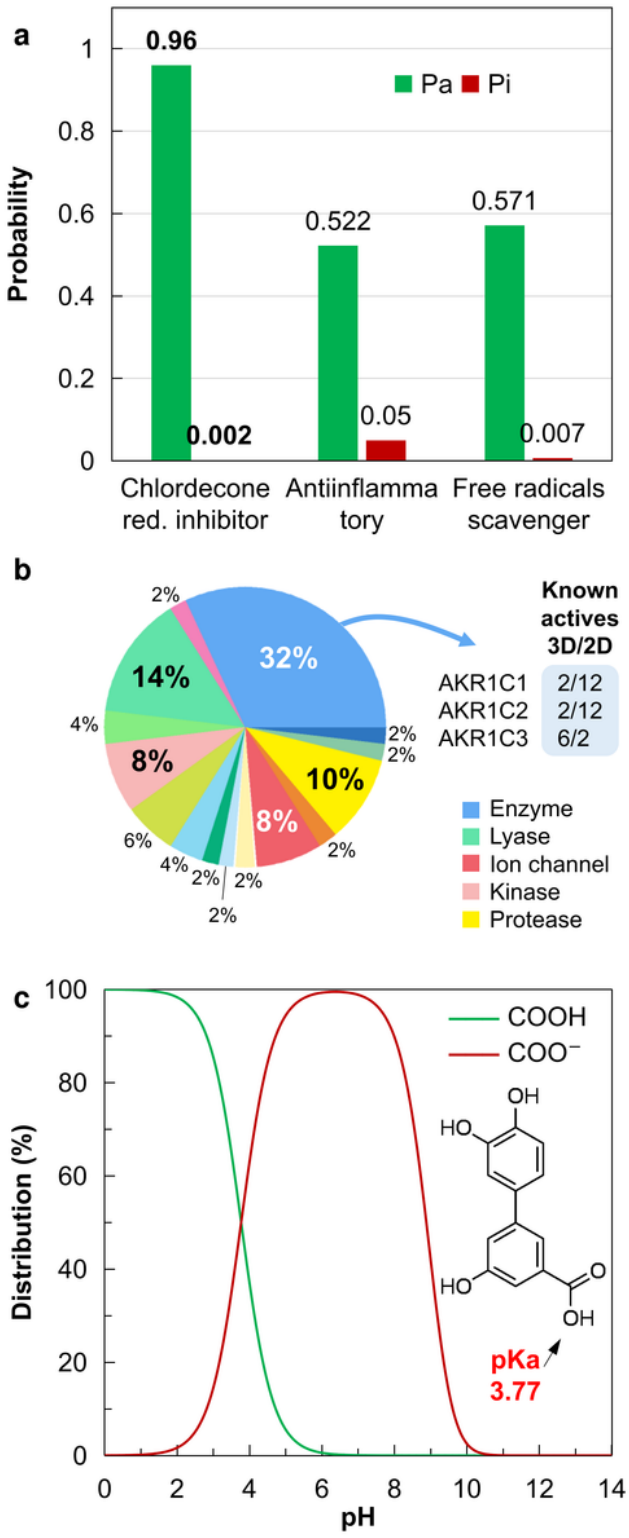

Figure 2

(A) Show the results of the PASS prediction to chlordecone reductase (as aldo-keto reductase in PDB ID:4JQ1) inhibition, anti-inflammatory activity and free radical scavenger, (B) Show the results of virtual screening of target classes, by the 3D/2D drug-similarity, and (C) show the microspecies distribution chart by the calculated pKa value of the carboxylate group.

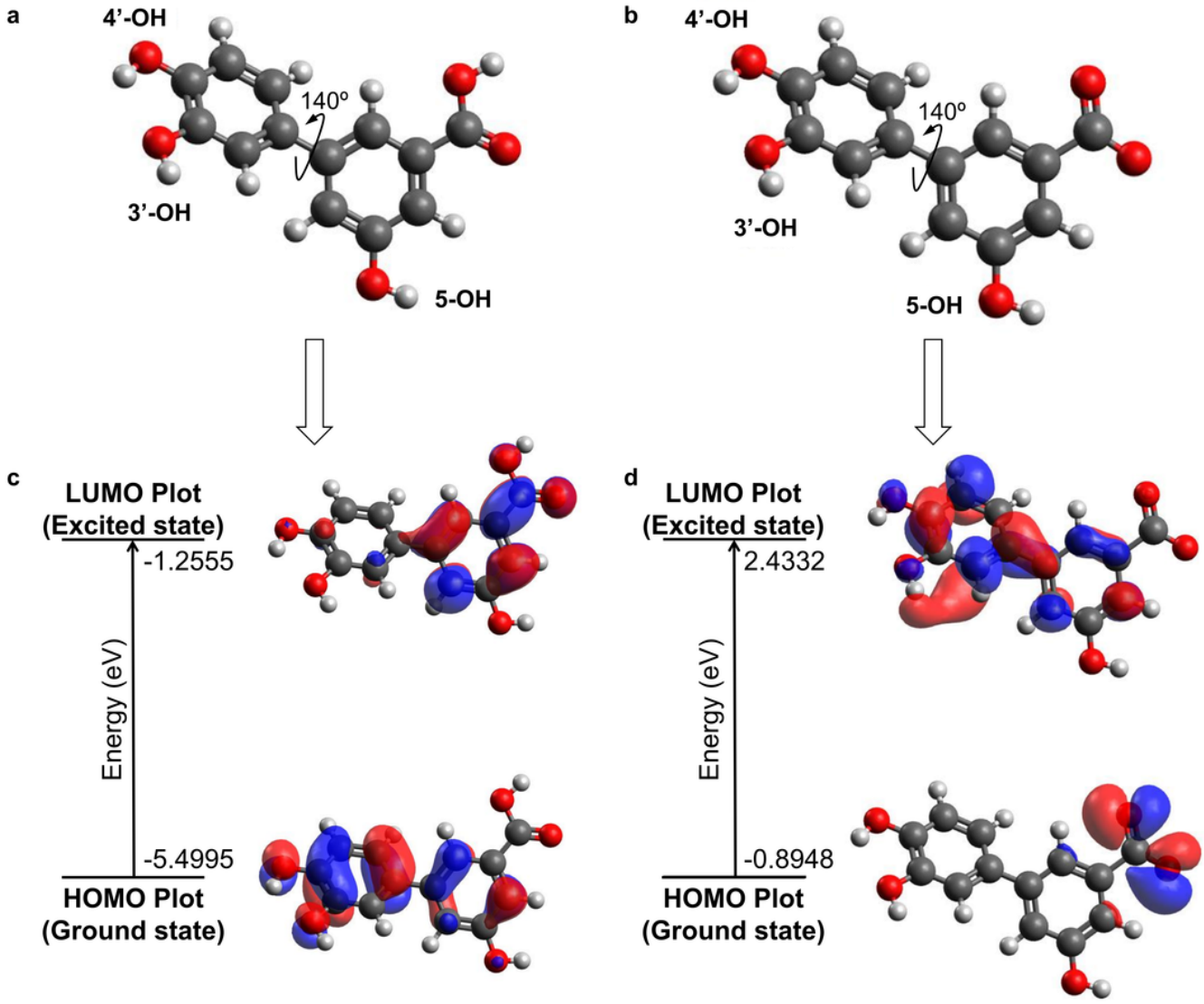

Figure 3

(A) Three-dimensional structure of the neutral species, (B) three-dimensional structure of the carboxylate anion of Castanol B optimized by MMFF94, (C) frontier orbitals HOMO and LUMO of the neutral species, and (D) frontier orbitals HOMO and LUMO of the conjugate base, optimized by DFT B3LYP/6-31G (d, p), generated by Marvin software and visualized by Avogadro *software*.

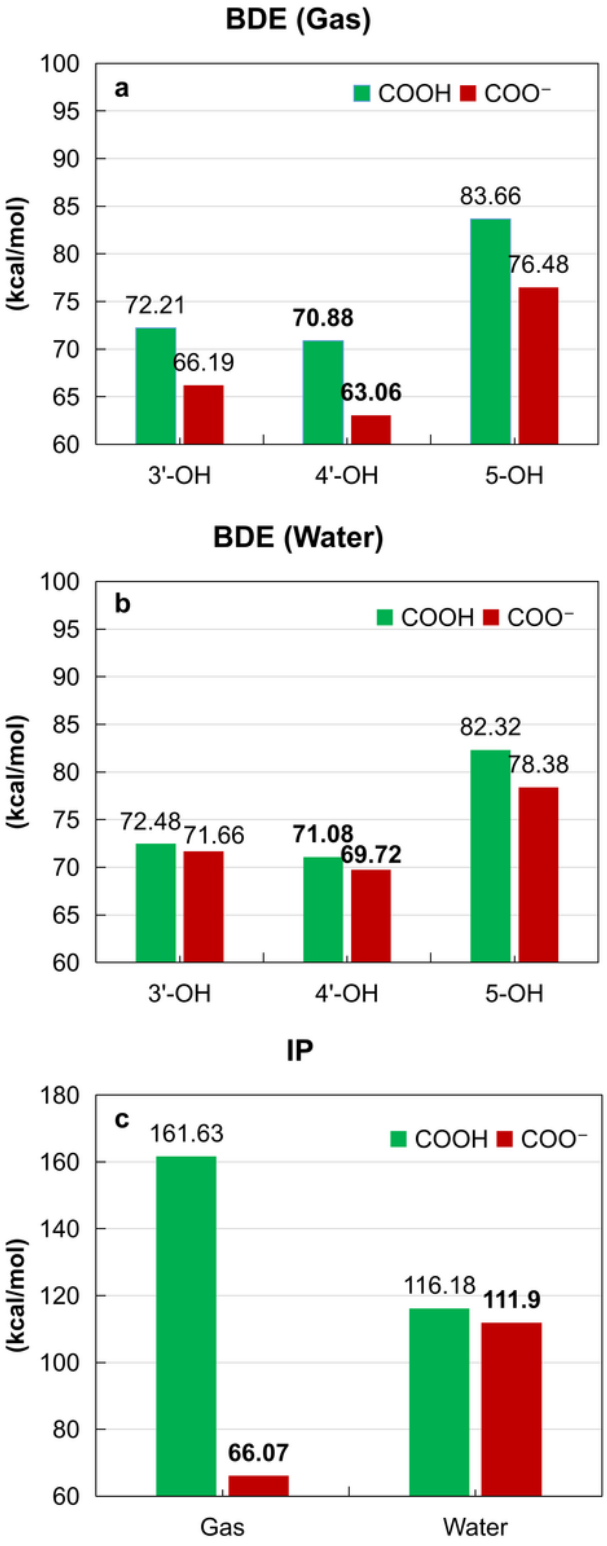

Figure 4

(A) BDE values for Castanol B (neutral and carboxylate anion) in gaseous form, (B) BDE values for Castanol B (neutral and carboxylate anion) in aqueous medium, and (C) IP values for Castanol B (neutral and carboxylate anion), in the gas phase and aqueous medium.

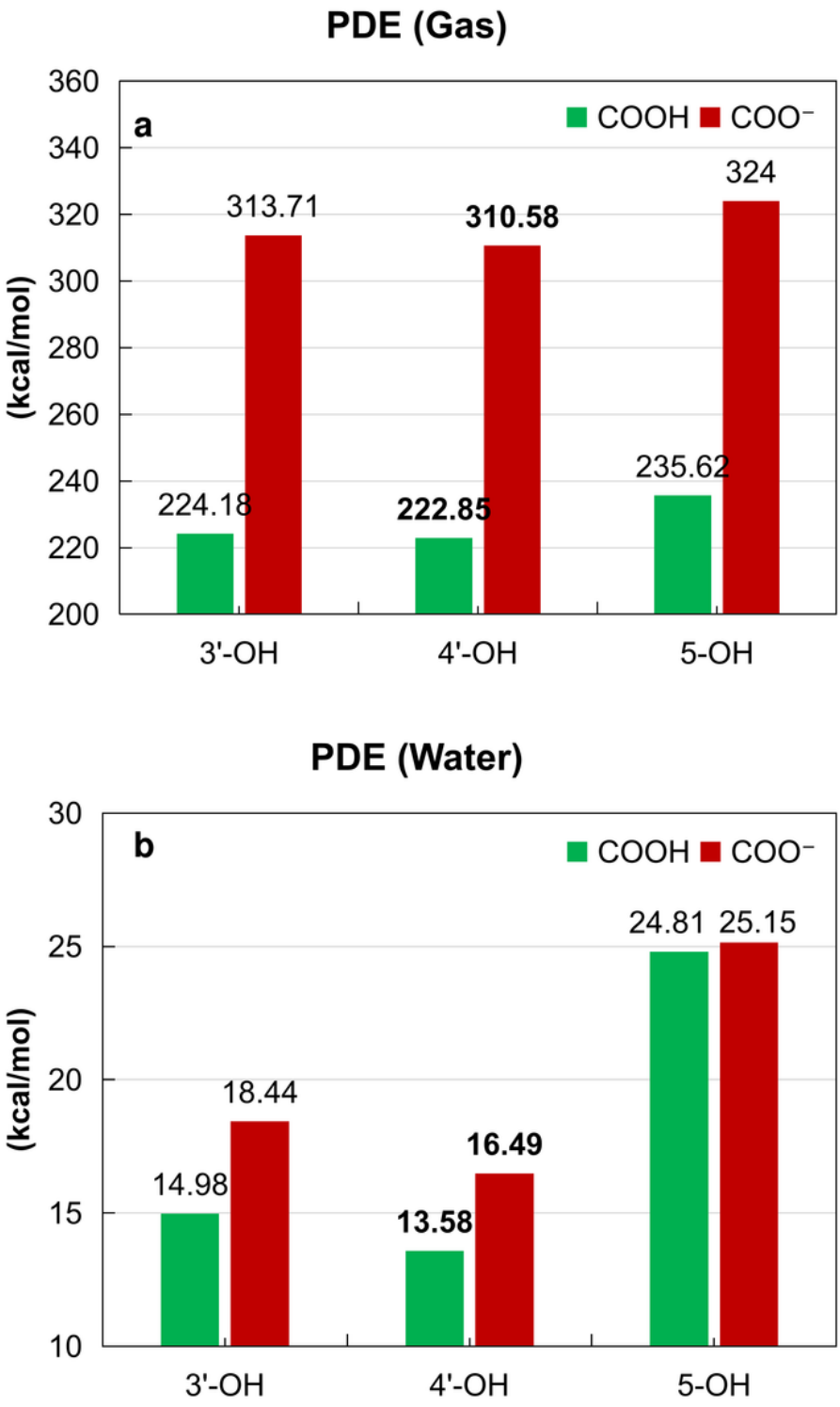

Figure 5

(A) Shows PDE values for Castanol B (neutral and carboxylate anion) in the gas phase and (B) shows PDE values for Castanol B (neutral and carboxylate anion) in the aqueous medium.

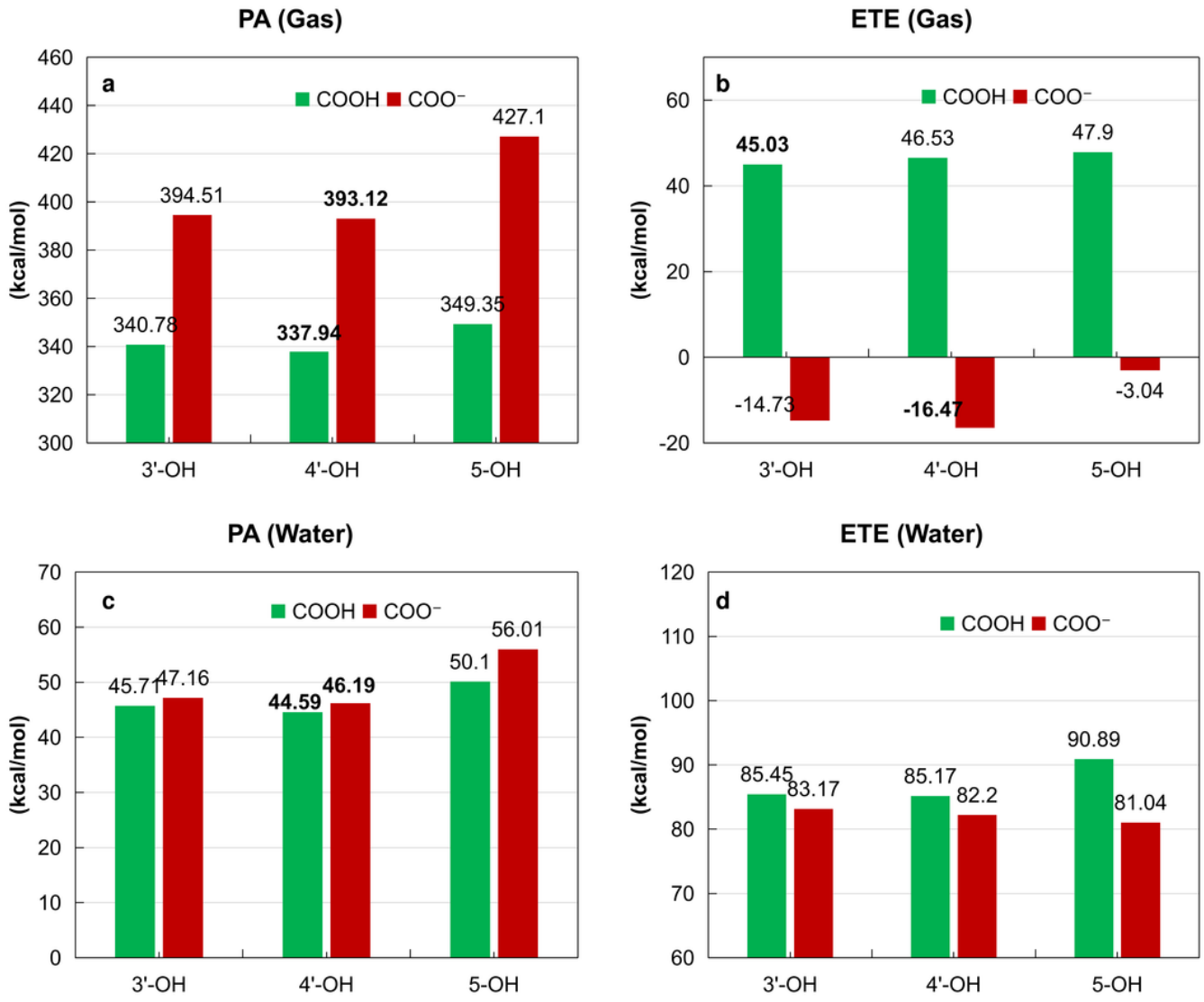

Figure 6

(A) and (B) show the PA and ETE values for Castanol B (neutral and carboxylate anion) in the gas phase, and (C) and (D) show the PA and ETE values for Castanol B (neutral and carboxylate anion) in the aqueous medium.

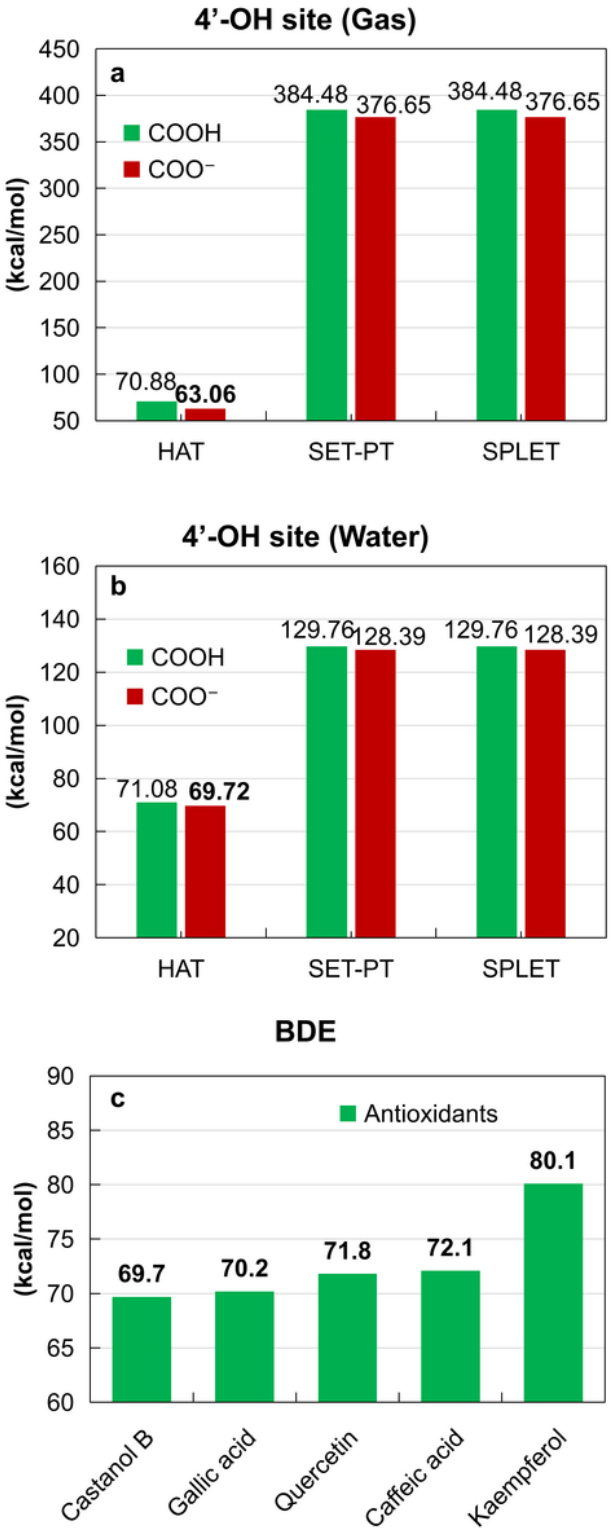

Figure 7

(A) Shows HAT, SET-PT and SPLET values at the 4'-OH site for Castanol B (neutral and carboxylate anion) in the aqueous medium, (B) shows the HAT, SET-PT and SPLET values at the 4'-OH site for Castanol B (neutral and carboxylate anion), in the aqueous medium, and (C) shows BDE values for Castanol B and the most studied antioxidants.

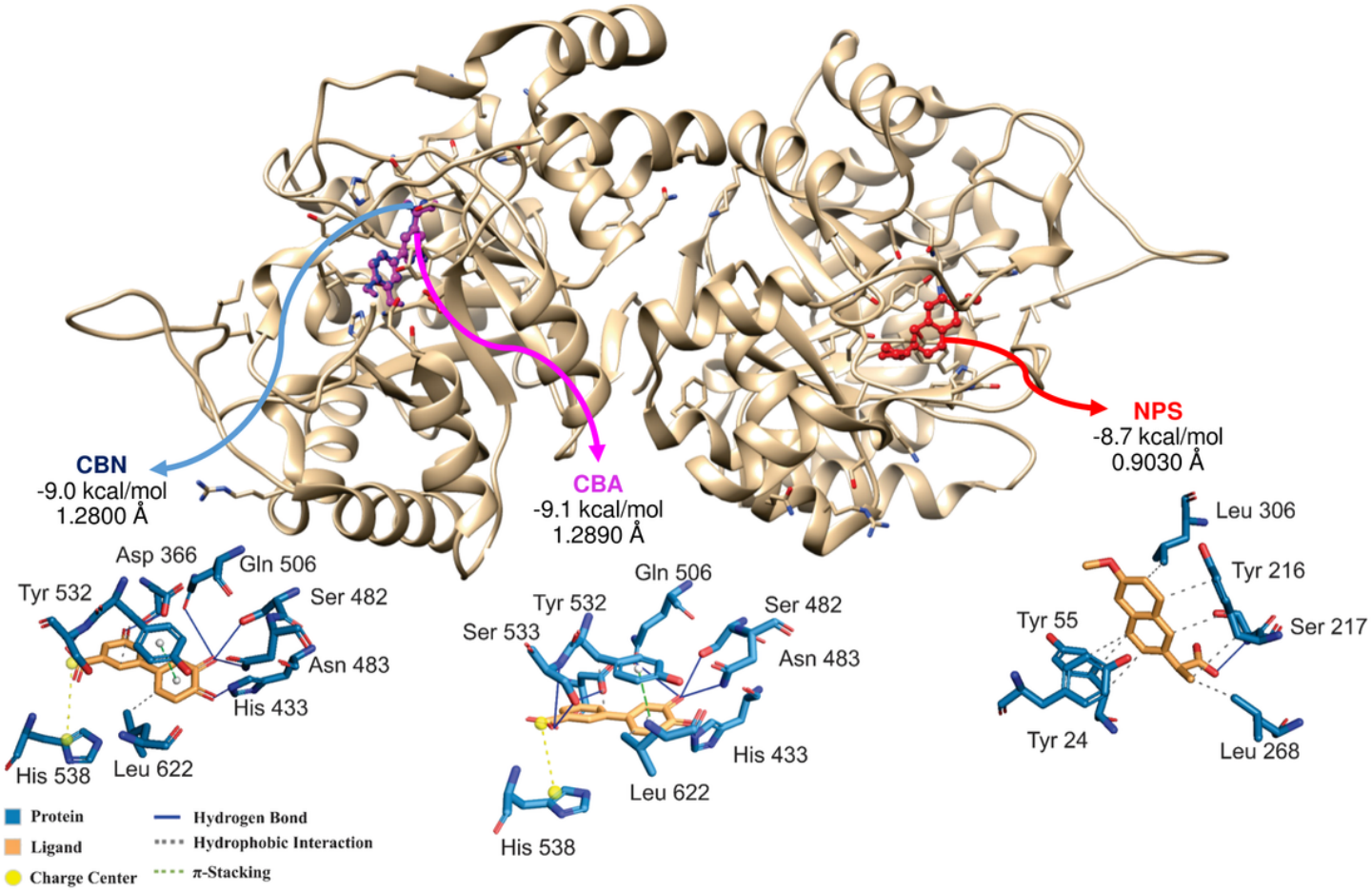

Figure 8

Affinity energy, RMSD values, and binding site between the AKR1C2 receptor with the NPS (red), CBN (blue), and CBA (magenta) ligands.

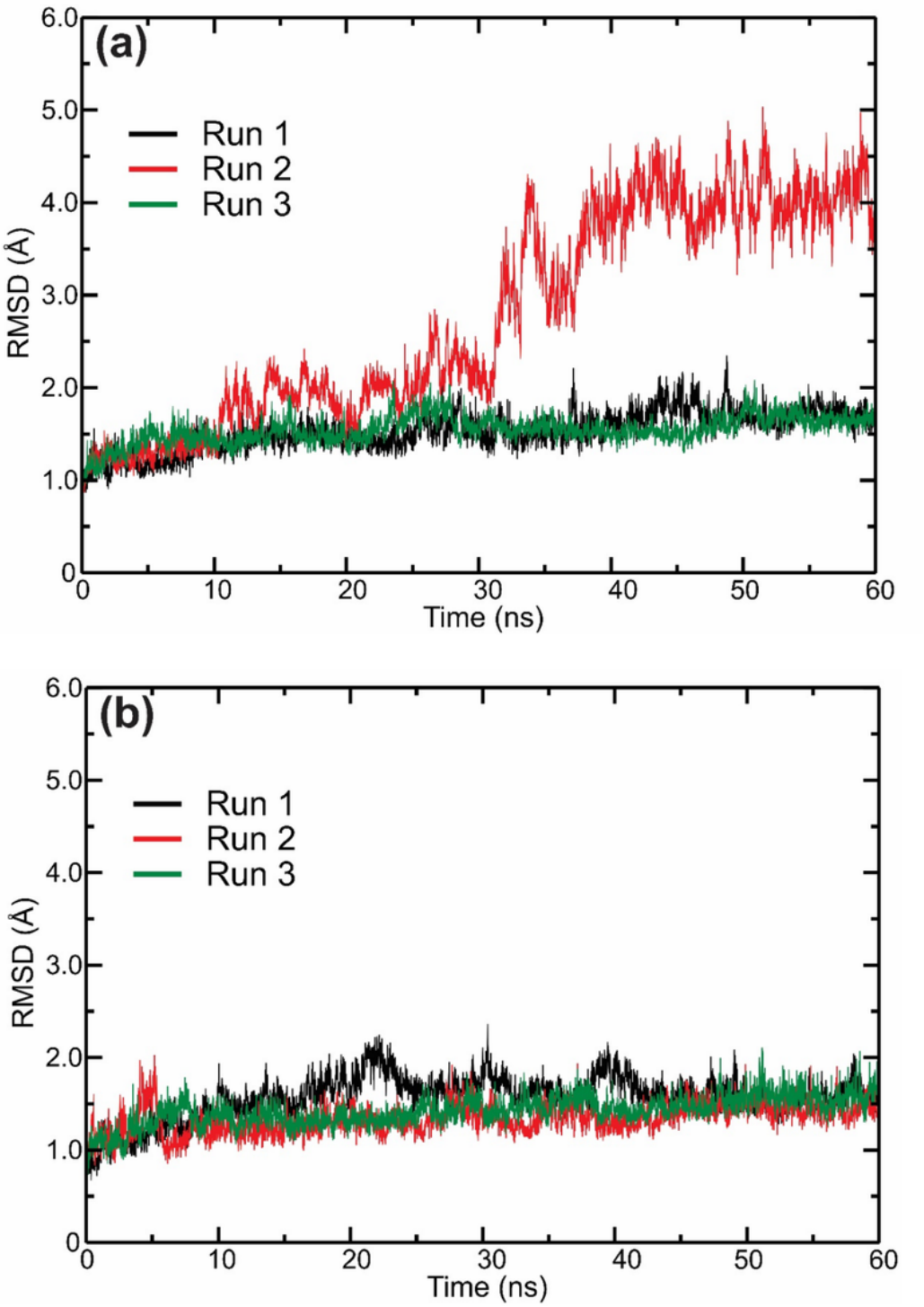

Figure 9

Determination of RMSD for the (A) AKR1C2-CBN and (B) AKR1C2-CBA complexes. The MD simulations were performed in three replicates (black, red, and green).

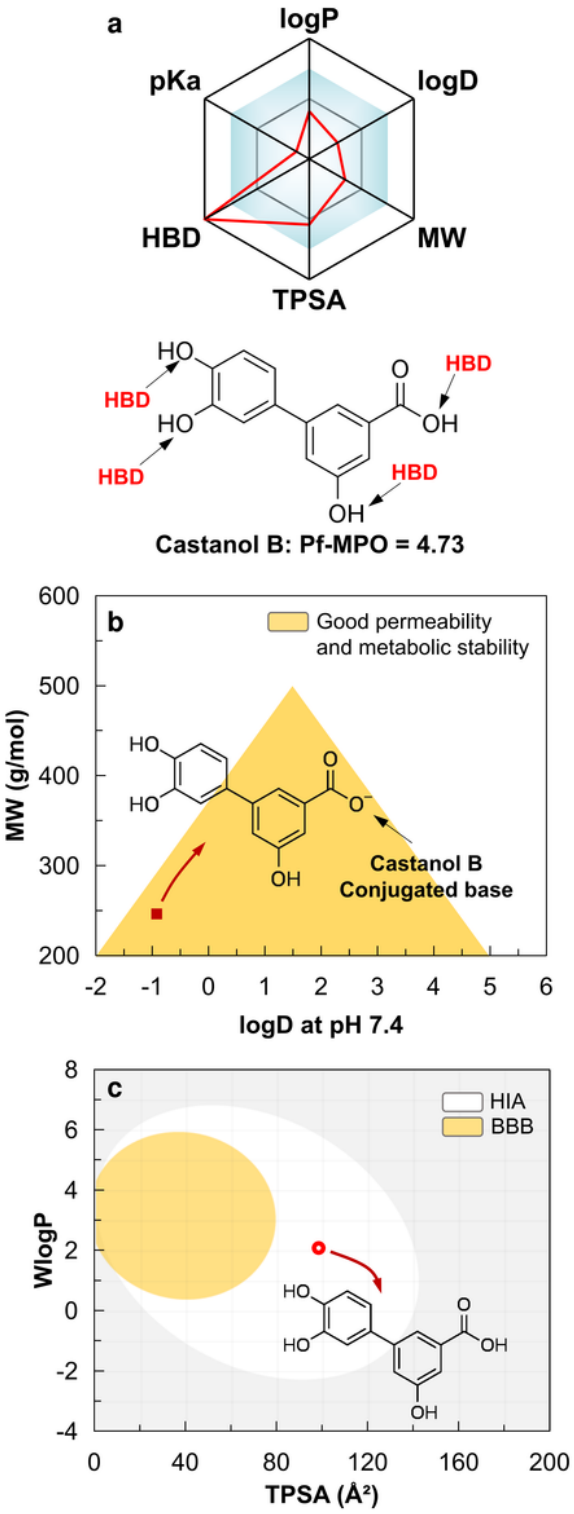

Figure 10

(A) Show the estimate of drug-space as a function of the major microspecie of the Castanol B, (B) is the druglikeness estimation by the Pf-MPO algorithm and (C) show the estimate brain and intestinal passive permeation.

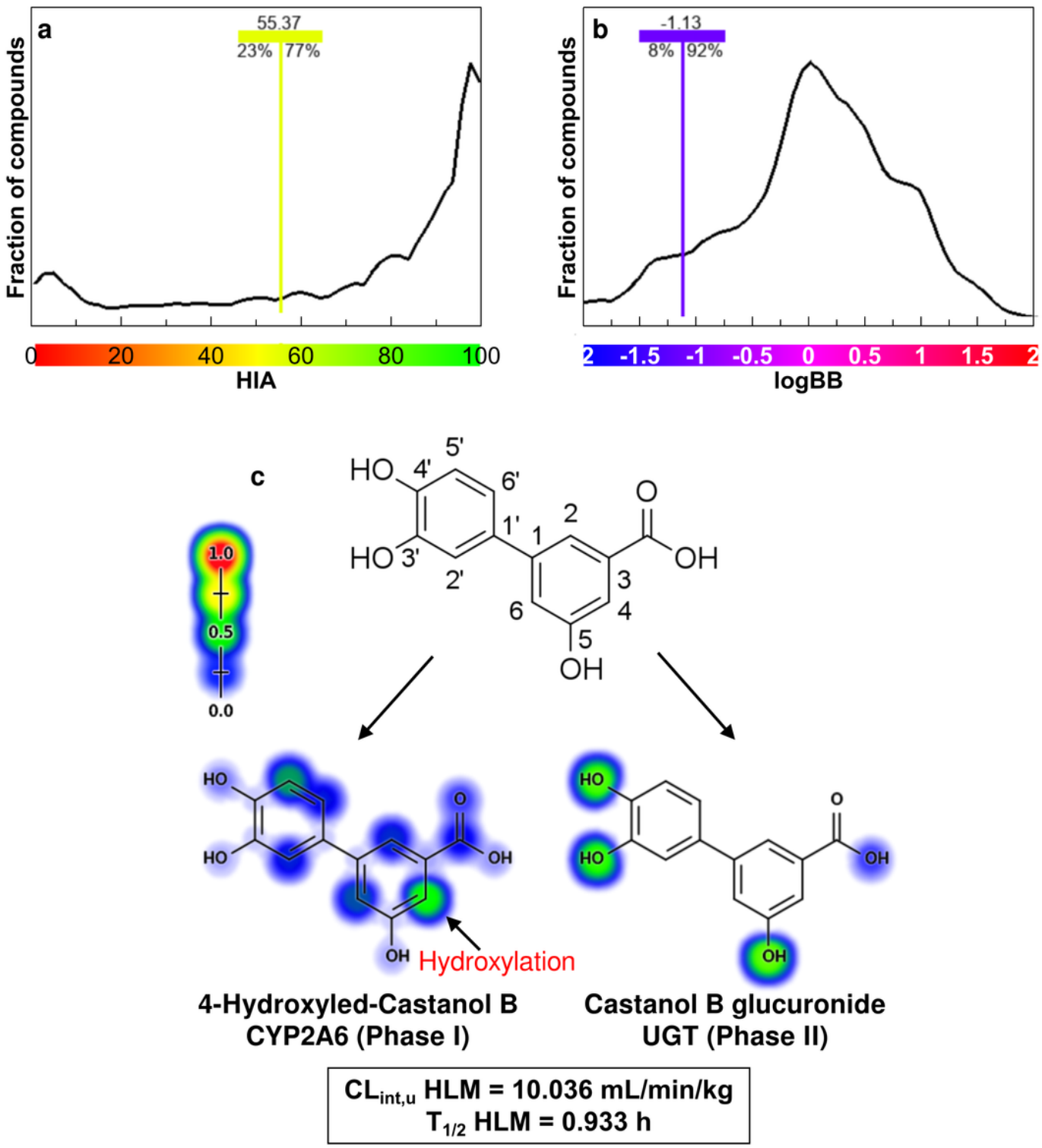

Figure 11

(A) Show the quantitative estimates of relative oral bioavailability, (B) show the permeability at BBB, and (C) show the structural contributions associated with phases I and II of metabolism of the Castanol B.

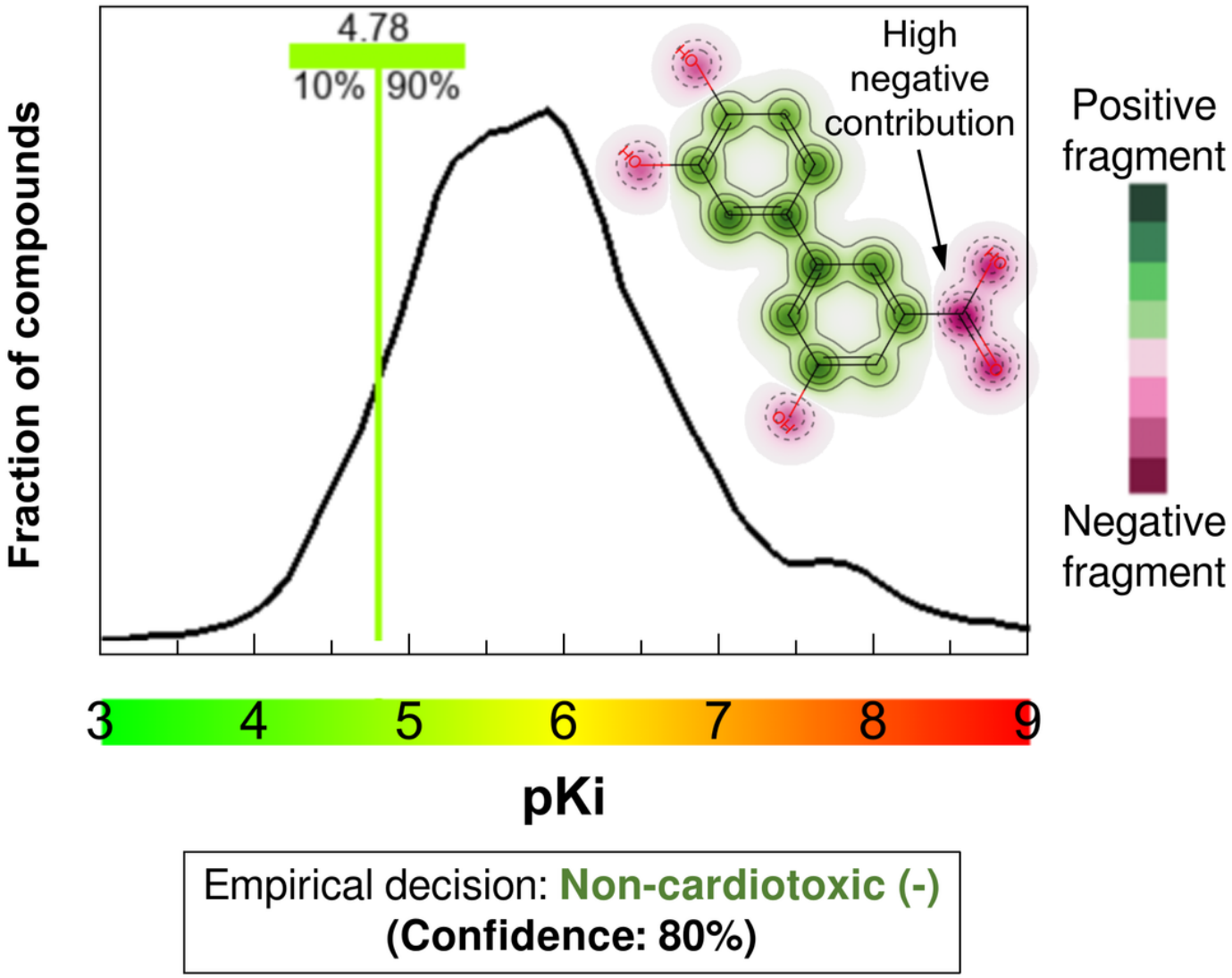

Figure 12

Show the Structural contributions of Castanol B to affinity (pKi) with hERG channels, where the carboxyl group constitutes a strong negative fragment (magenta color) and the aromatic rings constitute hydrophobic interactions (green color) that prevent the blocking of hERG channels.

Supplementary Files

This is a list of supplementary files associated with this preprint. Click to download.

- Electronicsupplementarymaterial.docx